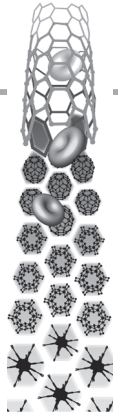

Efficient systemic delivery of siRNA by using high-density lipoprotein-mimicking peptide lipid nanoparticles

The main challenge for RNAi therapeutics lies in systemic delivery of siRNA to the correct tissues and transporting them into the cytoplasm of targeted cells, at safe, therapeutic levels. Recently, we developed a high-density lipoprotein-mimicking peptide–phospholipid scaffold (HPPS) and demonstrated its direct cytosolic delivery of siRNA *in vitro*, thereby bypassing endosomal trapping. **Aim:** We investigate the *in vivo* implementation of HPPS for siRNA delivery. **Method & results:** After systemic administration in KB tumor-bearing mice, HPPS prolonged the blood circulation time of cholesterol-modified siRNA (chol-siRNA) by a factor of four, improved its biodistribution and facilitated its uptake in scavenger receptor class B type I overexpressed tumors. For therapeutic targeting to the *bcl-2* gene, the HPPS-chol-si-bcl-2 nanoparticles downregulated Bcl-2 protein, induced enhanced apoptosis (2.5-fold) in tumors when compared with controls (saline, HPPS, HPPS-chol-si-scramble and chol-si-bcl-2) and significantly inhibited tumor growth with no adverse effect. **Conclusion:** HPPS is a safe, efficient nanocarrier for RNAi therapeutics *in vivo*.

Original submitted 2 December 2011; Revised submitted 19 April 2012

KEYWORDS: bcl-2 ■ cytosolic delivery ■ high-density lipoprotein ■ nanoparticle ■ siRNA ■ SR-BI

Qiaoya Lin[1,2,3], Juan Chen[1], Honglin Jin[1,2,3], Kenneth K Ng[1,4], Mi Yang[1,5], Weiguo Cao[1,6], Lili Ding[1], Zhihong Zhang[1,3] & Gang Zheng*[1,2,4]

[1]Ontario Cancer Institute and Techna Institute, University Health Network, Toronto, Canada
[2]Department of Medical Biophysics, University of Toronto, Toronto, Canada
[3]Britton Chance Center for Biomedical Photonics, Wuhan National Laboratory for Optoelectronics-Huazhong University of Science & Technology, Wuhan, China
[4]Institute of Biomaterials & Biomedical Engineering, University of Toronto, Toronto, Canada
[5]Department of Oncology, Drum Tower Hospital Affiliated to School of Medicine & Clinical Cancer Institute of Nanjing University, Nanjing, China
[6]Department of Chemistry, Shanghai University, Shanghai, China
**Author for correspondence:*
Tel.: +1 416 581 7666
Fax: +1 416 581 7667
gang.zheng@uhnres.utoronto.ca

RNAi therapeutics have been hailed as the personalized medicine of the future and have shown early promise in clinical trials [1,2]. However, challenges remain in systemic delivery of the siRNA to the correct tissues and transporting them into the cytoplasm of targeted cells, at safe, therapeutic levels. To address these issues, one approach is to improve the *in vivo* stability of siRNA via backbone modification through, for example, 2′fluoropyrimidine, 2′-*O*-methyl and phosphorothioate modification, or via cholesterol labeling, amongst other techniques [3–7]. Another approach is to develop desirable systemic delivery strategies to shield siRNAs from kidney filtration, phagocyte uptake and enzymatic degradation, and further efficiently transport siRNA into the cytoplasm of targeted cells where siRNAs are recognized and associated with the RNA-induced silencing complex to perform their gene knockdown function. So far, a wide range of systemic vehicles have been developed to address some of these critical challenges, such as polymers, cationic lipids and liposomes [1,2,8–18], but further improvements are warranted, particularly with regards to toxicity and efficiency of cytosolic delivery. Recently, delivery systems based on natural, endogenous nanoparticles, such as lipoproteins and exosomes [19–23], have gained increasing attention because of their biocompatibility and unique transport pathways. In particular, high-density lipoproteins (HDLs) with their small size profile (5–12 nm), long circulation half-life (15 h) and the capability of offloading its cholesterol ester content directly into the cytoplasm of cells via its interaction with the scavenger receptor class B type I (SR-BI) receptor [24] are attractive for siRNA delivery. In fact, some RNAi therapeutics based on HDL or reconstituted HDLs (rHDLs) have been introduced and the improvement in gene silencing in multiple animal models via SR-BI targeting has been validated [25–27]. We recently developed a HDL-mimicking peptide–phospholipid nanoscaffold (HPPS) nanoparticle composed of the cholesteryl oleate, phospholipid and an 18-amino acid apolipoprotein A-I (ApoA-1) mimetic peptide [28]. The potential clinical translation advantage of using this peptide over the plasma-derived or recombinant full-length ApoA-1 protein is to address the challenges relating to the protein's large-scale production, purity and cost. The HPPS nanoparticle closely mimics the structural and functional properties of plasma-derived HDL. The nanoparticle has a monodisperse size (<30 nm), long circulation half-life (15 h) and excellent biocompatibility confirmed by its tolerability at a systemic administration of 2000 mg/kg of HPPS [28,29]. More importantly, we have demonstrated that HPPS is capable of delivering

Future Medicine part of fsg

cholesterol-modified siRNA (chol-siRNA) directly into the cytosol of the target cells *in vitro* via the SR-BI receptor, thereby bypassing the detrimental endosomal trapping and resulting in enhanced gene silencing efficacy [30]. Here, we report on the successful *in vivo* systemic delivery of siRNA to tumor cells using HPPS nanoparticles, resulting in a significant siRNA-mediated tumor growth inhibition without adverse effects, thus demonstrating the utility of HPPS as a safe and efficient nanocarrier for RNAi therapeutics.

Materials & methods

Materials

1, 2-dimyristoyl-sn-glycero-3-phosphocholine was purchased from Avanti Polar Lipids Inc. (AL, USA). Anti-β-actin antibody and cholesteryl oleate was obtained from Sigma-Aldrich Co. (MO, USA). The ApoA-1 mimetic, amphipathic α-helical peptide, Ac-FAEKFKEAVKDYFAKFWD, was purchased from GL Biochem Ltd. (Shanghai, China). All siRNAs were synthesized by Genepharma Co. (Shanghai, China). Cholesterol-conjugated siRNA-bcl-2 (chol-si-bcl-2) consisted of the sense strand 5′-chol-GfUGAAGfUfCAAfCAfUGfCfCfUGfC-dTsdTs-3′ and antisense strand 5′-GfCAGGfCAfUGfUfUGAfCfUfUfCAfC-dTsdT-3′. Cholesterol-conjugated siRNA bearing a scrambled sequence (chol-si-scramble) consisted of the sense strand 5′-chol-GAfCGfUAAfCGGfCfCAfUAGfUfCfU-dTsdTs-3′ and the antisense strand 5′-AGAfCfUAfUGGfCfCGfUfUAfCGfUfC-dTsdT-3′. Cy5.5-labeled cholesterol-conjugated mock siRNA (Cy5.5-chol-siRNA) was modified by the same method as chol-si-bcl-2, and the dye Cy5.5 was labeled on the antisense strand 5′ (abbreviations as follows: chol, cholesterol; fC and fU, 2′-deoxy-2′-fluoro cytidine and uridine, respectively; 's', phosphorothioate linkage). The (Z)-octadec-9-enyl 2-(3-((Z)-octadec-9-enyloxy)-6-oxo-6H-xanthen-9-yl) benzoate or Dioleyl Fluorescein (Fluo-BOA) was synthesized by the previously reported methods [31]. Anti-Bcl-2 antibody, antirabbit secondary antibody and LumiGLO® kit were all purchased from Cell Signaling Technology (MA, USA). Agarose (electrophoresis grade) was obtained from BioShop Canada Inc. (Burlington, Canada). KB (SR-BI$^+$), HT1080 (SR-BI$^-$) cell lines and cell culture media Eagle's Minimum Essential Medium were obtained from the American Type Culture Collection. The fetal bovine serum, trypsin-EDTA solution and Hoechst 33258 were all purchased from Gibco-Invitrogen Co. (CA, USA).

Nanoparticles preparation

HPPS and Fluo-BOA-labeled HPPS (HPPS[Fluo-BOA]) were prepared and purified as previously described [28]. Chol-si-bcl-2, chol-si-scramble and Cy5.5-chol-siRNA were dissolved in RNase-free water to make 250 μM solutions. The Cy5.5-chol-siRNA solution and HPPS(Fluo-BOA) were combined and mixed at a 10:1 molar ratio and incubated for 1 h at room temperature. The mixture was then purified by FPLC to remove free Cy5.5-chol-siRNA and acquire HPPS(Fluo-BOA)-Cy5.5-chol-siRNA nanoparticles (Supplementary Figure 1, see online at www.futuremedicine.com/doi/suppl/10.2217/nnm.12.73). HPPS-chol-si-bcl-2, HPPS-chol-si-scramble and HPPS-Cy5.5-chol-siRNA nanoparticles were prepared using the same method for *in vivo* study.

Characterization of HPPS(Fluo-BOA)-Cy5.5-chol-siRNA

Determination of nanoparticle compositions

The HPPS concentration was determined using the previously reported method [32] and the concentration of siRNA was quantified by measuring its absorbance at 260 nm by Varian Cary 50 UV-visible spectrophotometer.

Morphology, size & ζ-potential measurement

Transmission electron microscopy was performed on a Hitachi H-7000 transmission electron microscope (Hitachi Inc., Japan) utilizing a digital image acquisition system to determine the size dispersion and morphology of HPPS(Fluo-BOA)-Cy5.5-chol-siRNA stained with 2% phosphotungstic acid. The particle size distributions of HPPS(Fluo-BOA) and HPPS(Fluo-BOA)-Cy5.5-chol-siRNA were measured by dynamic light scattering (Zetasizer Nano-ZS90; Malvern Instruments, UK) using a 4.0 mW He-Ne laser and operating at 633 nm with a detector angle of 90°. The ζ-potential of HPPS(Fluo-BOA) and HPPS(Fluo-BOA)-Cy5.5-chol-siRNA were measured using patented M3-PALS technology (Zetasizer Nano-ZS90).

Gel shift assay

HPPS(Fluo-BOA), HPPS(Fluo-BOA)-Cy5.5-chol-siRNA and Cy5.5-chol-siRNA were loaded into a 2% agarose gel containing 0.002% (v/v) Gel red. The 2 μg of Cy5.5-chol-siRNA was loaded per well, while HPPS(Fluo-BOA) amount was kept constant. The gel was run at 100 V for 45 min and subsequently imaged by UV transillumination and by the Maestro™-CRi imaging system

(Caliper Life Sciences Inc., MA, USA). HPPS was visualized by Fluo-BOA fluorescence using the blue filter set (excitation filter: 445–490 nm; emission filter: 515 nm long pass; signal collection from 500–650 nm in a 10 nm-step) and siRNA was visualized by Cy5.5 fluorescence using the red filter set (excitation filter: 615–665 nm; emission filter: 700 nm long pass; signal collection from 680–950 nm in 10 nm-step).

To check the stability of nanoparticles in serum, HPPS(Fluo-BOA)-Cy5.5-chol-si-RNA and Cy5.5-chol-siRNA were incubated with 10% mouse serum at 37°C for 1, 2, 4 and 6 h, respectively. The samples were then analyzed by electrophoresis using 2% agarose gel to monitor the release or degradation of nanoparticles. Images were taken using the same method as described above.

Confocal microscopy of HPPS(Fluo-BOA)-Cy5.5-chol-siRNA *in vitro*

KB and HT1080 cells (4×10^4 per well) were seeded into eight-well cover-glass-bottom chambers (Nunc Lab-Tek, Sigma-Aldrich) and incubated for 24 h at 37°C in an atmosphere of 5% CO_2 in a humidified incubator. HPPS(Fluo-BOA)-Cy5.5-chol-siRNA was then added into the chamber wells at a siRNA concentration of 200 nM, and for the HDL-blocking group, an excess of HDL was added into chamber wells 15 min before HPPS(Fluo-BOA)-Cy5.5-chol-siRNA. After a 3 h incubation, KB cells and HT1080 cells were washed twice with PBS and replaced with fresh cell culture medium, and Hoechst 33258 (1 µl, 5 mM) was added to each well for nucleus staining. The confocal image of the cells was taken by Olympus FV1000 laser confocal scanning microscopy (Olympus, Tokyo, Japan) with excitation wavelengths of 488 nm (exciting Fluo-BOA), 405 nm (exciting Hoechst 33258) and 633 nm (exciting Cy5.5).

Xenograft model in nude mice

All animal studies were conducted in the Animal Resource Center of the University Health Network in accordance with protocols approved by the Animal Care Committee. Nude mice (female, 7–8 weeks old) were inoculated with 2×10^6 KB cells (in 100 µl PBS) subcutaneously in the right flanks.

Whole-body fluorescence imaging

KB xenograft tumor-bearing mice were intravenously injected with HPPS-Cy5.5-chol-siRNA or Cy5.5-chol-siRNA at a Cy5.5-chol-siRNA dose of 1 mg/kg. Whole-body fluorescence images were taken before injection at 5 min, 30 min, 1, 3, 6, 9 and 24 h postinjection using the CRI Maestro imaging system with a red filter set (excitation filter: 615–665 nm; emission filter: 700 nm long pass; signal collection from 680–950 nm in 10 nm-step) and an exposure time of 1000 ms.

Ex vivo tissue fluorescence imaging

After imaging, mice were sacrificed, and organs and tumor tissues were excised, washed with PBS and imaged using the Maestro imaging system. Subsequently, all the tissues were frozen in liquid nitrogen and then cut into slides of 5 µm thickness using a Leica CM3050S cryostat. The slides were imaged by Olympus FV1000 laser confocal scanning microscopy with an excitation wavelength of 633 nm.

Blood clearance of nanoparticles

Eight healthy nude mice were used for determining the blood clearance of nanoparticles. Mice were randomly allocated into two groups. Mice in group A (n = 4) were administered intravenously with Cy5.5-chol-siRNA at a dose of 1 mg/kg, and mice in group B (n = 4) were administered intravenously with HPPS-Cy5.5-chol-siRNA at the same Cy5.5-chol-siRNA dose. Blood was collected before injection and 5 min, 30 min and 1, 2, 4, 6 and 8 h postinjection. After the blood samples were completely clotted, they were centrifuged at full speed (12,000 rpm) for 10 min at room temperature to isolate blood serum. The serum was diluted with PBS and detected for Cy5.5 fluorescence on HORIBA FluoroMax-4 spectrofluorometer (HORIBA Scientific, NJ, USA; excitation: 650 nm; emission: 670–690 nm). The concentration of Cy5.5-chol-siRNA in blood was then calculated based on its fluorescence stand curve, which was generated by measuring the fluorescence of the blood serum with known amounts of Cy5.5-chol-siRNA.

In vivo therapeutic efficacy of HPPS-cho-si-bcl-2

Twenty four KB xenograft tumor-bearing mice were used in the therapeutic study. Mice were subjected to treatment when the tumor volume reached 40–50 mm^3 on day 10 after the inoculation. They were randomly assigned to five treatment groups. Mice were administered intravenously with saline (group 1; n = 6), HPPS (group 2; n = 3), HPPS-chol-si-scramble (group 3; n = 3), chol-si-bcl-2 (group 4; n = 6) and HPPS-chol-si-bcl-2 (group 5; n = 6),

doi:10.2217/NNM.12.73

respectively. Each treatment group received tail vein injections of the following dose every other day for a total two doses: saline (200 µl), HPPS (57.3 nmol/kg in 200 µl saline), HPPS-chol-si-scramble (containing 8 mg/kg of siRNA and 57.3 nmol/kg of HPPS in 200 µl saline), chol-siRNA (8 mg/kg siRNA in 200 µl saline), HPPS-chol-si-bcl-2 (containing 8 mg/kg of siRNA and 57.3 nmol/kg of HPPS in 200 µl saline). All the mice were sacrificed on day 14, and variable organs and tumor tissues were excised and quickly frozen in liquid nitrogen until used.

Western blotting

Frozen tumor tissues (20–30 mg) were cut, transferred to glass tubes and homogenized with 0.5 ml ice-cold lysis buffer as previously described [30]. The homogenate was incubated in an ice bath for 15–60 min to lyse the cells, and then centrifuged at 10,000–15,000 g (4°C) for 20 min to pellet cellular debris. The supernatant-containing protein was collected in fresh tubes and the concentration of protein was determined by a Bradford protein assay. Samples were diluted at 1:2 with working buffer (50 µl β-mercaptoethanol + 950 µl sodium dodecyl sulfate reducing buffer) and were denatured at 95°C for 4 min. 5 µg of KB tumor tissue protein from different groups were loaded in wells on a sodium dodecyl sulfate polyacrylamide gel (containing 10% resolving gel and 4% stacking gel) and the gel was run at 120 V for 2–3 h. The samples were then transferred to polyvinyl difluoride membrane by standard method. After transfer, the polyvinyl difluoride membrane was washed with 25 ml TBS for 5 min at room temperature and incubated in 25 ml of blocking buffer for 1 h at room temperature with gentle agitation (blocking buffer: TBS, 5% w/v nonfat dry milk, 0.1% Tween-20). The membrane was then washed three times for 5 min each with 15 ml TBS/T (TBS, 0.1% Tween-20) and incubated with anti-Bcl-2 rabbit polyclonal primary antibody in 10 ml primary antibody (1:1000) dilution buffer with gentle agitation overnight at 4°C. The membrane was washed as previously described and then incubated with HRP-conjugated goat antirabbit secondary antibody (1:2000) and HRP-conjugated anti-β-actin antibody (1:10000) in 10 ml of blocking buffer for 1 h. The membrane was washed three times for 5 min each with 15 ml TBS/T. The protein was visualized using LumiGLO reagent (Cell Signaling Technology, USA) and Typhoon 9410 variable-mode imager (GE Healthcare, NJ, USA). The data was quantified by Image J software (Wayne Rasband, NIH).

Terminal deoxynucleotidyl transferase dUTP nick end labeling assay

Terminal deoxynucleotidyl transferase dUTP nick end labeling (TUNEL) assay was performed on frozen sections using an *in situ* end-labeling technique for apoptosis as previously reported [33]. Slides were fixed with 1% PFA in PBS, pH 7.4 preferably for 10 min at room temperature. After draining off excess liquid and washing twice with PBS (5 min each), slides were postfixed in precooled ethanol:acetic acid (2:1) for 5 min at -20°C. The ethanol: acetic acid mixture was removed and slides were washed with two changes of PBS. Endogenous peroxidase activity was blocked using 3% aqueous hydrogen peroxide and endogenous biotin activity using avidin/biotin blocking kit (Lab Vision Cat.# TA-015-BB). Sections were treated with buffer A (50 mM TRIS-HCl [pH 7.5], 50 mM $MgCl_2.6H_2O$, 100 mM β-mercaptoethanol and 0.005% BSA) for 5–10 min and then were incubated with a biotin-nucleotide cocktail in a water bath at 37°C for 1.5 h. After washing with PBS, slides were labeled with Ultra Streptavidin Horseradish Peroxidase Labeling Reagent (ID Labs inc. Cat.# BP2378) for 30 min at room temperature. The slides were then developed with freshly prepared DAB (Dako K3468) and counterstained with Mayer's hematoxylin. Last, the slides were dehydrated and mounted. Slides were scanned by Aperio Whole Slide Scanner and analyzed by Aperio ImageScope. The cells showing the DAB staining positive and with the morphology of cytoplasmic condensation, loss of cell–cell contact and shape of shrinkage were counted as TUNEL positive cells.

In vivo antitumor activity

Tumor dimensions were measured with vernier calipers and volumes were calculated as follows: tumor volume (mm^3) = width^2 (mm^2) × length (mm)/2. Tumor dimension was measured on day 10 before treatment, day 12 and 14 after treatment. All measurements were conducted in a blinded fashion.

In vivo adverse effects of HPPS-chol-si-bcl-2

To assess the adverse effects of HPPS-chol-si-bcl-2 during treatment, four healthy BALB/c mice (female, 6–7 weeks old) were administered intravenously with 10 mg/kg HPPS-chol-si-bcl-2 (based on chol-si-bcl-2 concentration) every 2 days and the other three mice were administered intravenously with 200 µl saline as controls. After injection, mice behaviors were monitored and the

body weight was measured every 2 days. Blood samples (200 µl per mouse) were collected from the saphenous vein to measure liver function and renal function by VetScan VS2 (Abaxis Inc., CA, USA) at 4 days post first injection, and then the mice were sacrificed and their organs (lung, heart, liver, spleen and kidney) were excised, fixed in 10% formalin, embedded in paraffin, sectioned and stained with hematoxylin and eosin for histological analysis.

Statistical analysis

The student's t-test (two tailed) was used to determine significant differences in Western blotting, TUNEL and *in vivo* antitumor activity. p-values less than 0.05 were considered significant.

Results

The integrity & stability of HPPS-chol-siRNA nanoparticles

The cytosolic delivery mechanism of chol-siRNA via HPPS has been validated previously [30]. To further investigate the integrity and intracellular fate of the HPPS-chol-siRNA particles, we developed a double-labeling approach where the core of HPPS was labeled with Fluo-BOA and the cholesterol-modified siRNA (chol-siRNA) was labeled with Cy5.5. To make the nanoparticles, HPPS(Fluo-BOA) was prepared first, and then loaded with Cy5.5-chol-siRNA as described in the method. After FPLC purification, a stable HPPS(Fluo-BOA)-Cy5.5-chol-siRNA nanoparticle was obtained (Supplementary Figure 1A). Loading Cy5.5-chol-siRNA on HPPS(Fluo-BOA) changed the surface charge and hydrodynamic diameter of the nanoparticles, evidenced by the ζ-potential shift from -2.1 ± 0.5 to -12 ± 0.5 mV and size change from 15.7 ± 0.3 to 21.0 ± 1.9 nm (determined by dynamic light scattering; Figure 1B & C), consistent with our previously reported HPPS-siRNA particles [30]. The size and spherical shape of the resulting HPPS(Fluo-BOA)-Cy5.5-chol-siRNA nanoparticles were further validated by transmission electron microscopy (Supplementary Figure 1B). Next, its integrity was determined by agarose gel electrophoresis photographed by UV illumination and dual fluorescence images. HPPS was visualized by Fluo-BOA fluorescence (blue filter, green color) and siRNA was visualized by Cy5.5 fluorescence (red filter, red color) using CRI Maestro imager. As shown in Figure 1D, the size and surface charge differences resulted in distinguishable gel migration of particles. HPPS(Fluo-BOA)-Cy5.5-chol-siRNA (lane 2) with both Fluo-BOA and Cy5.5 fluorescence moved faster than HPPS(Fluo-BOA) (lane 1) visualized only by Fluo-BOA fluorescence, but slower than free Cy5.5-chol-siRNA (lane 3) shown only by Cy5.5 fluorescence. The well-merged Fluo-BOA and Cy5.5 signals on lane 2 indicated the HPPS can stably carry chol-siRNAs by forming intact particles. The cholesterol labeling of siRNA plays a key role in the stable association of siRNA on the HPPS nanoparticles, which is consistent with our previous observation of low-density lipoprotein-mediated siRNA delivery where siRNA without cholesterol modification could not associate with low-density lipoprotein at all [20]. In nature, HDLs have the capacity of loading and offloading cholesterol to transfer cholesterol between cells and other lipoproteins. HPPS mimic HDL in both structural and functional property, thus we speculate that HPPS delivery of chol-siRNA is similar to HDL loading and offloading of cholesterol.

To further elucidate the intracellular fate of HPPS-chol-siRNA, confocal studies were performed on KB (SR-BI$^+$) and HT1080 cells (SR-BI$^-$). As shown in Figure 1E, both the HPPS core (the Fluo-BOA signal) and chol-siRNA (the Cy5.5 signal) were transported into the cytoplasm of KB cells (SR-BI$^+$), suggesting the preservation of HPPS-chol-siRNA integrity before it enters into cells and the similar intracellular delivery mechanism for both the siRNA and core payload of HPPS. In addition, adding a 50-fold excess of HDL significantly decreased both Cy5.5 and Fluo-BOA signals indicating that the cytosolic delivery of siRNA and HPPS core was efficiently blocked by HDL competition (Supplementary Figure 1C). Moreover, very little uptake of Cy5.5-chol-siRNA and Fluo-BOA was observed in HT1080 cells (SR-BI$^-$) (Supplementary Figure 1C). Taken together, these data demonstrate that the HPPS core payload and siRNA payload were both transported into the cytoplasm of cells by a SR-BI-mediated uptake pathway and the integrity of HPPS(Fluo-BOA)-Cy5.5-chol-siRNA during cell culture condition was maintained. After validating the integrity of HPPS(Fluo-BOA)-Cy5.5-chol-siRNA, we next investigated its stability in physiological conditions. HPPS(Fluo-BOA)-Cy5.5-chol-siRNA and free Cy5.5-chol-siRNA was incubated with 10% mouse serum at 37°C for different time durations and its stability was examined by agarose gel electrophoresis. The results showed that Cy5.5-chol-siRNA delivered by HPPS was stable up to 6 h (Supplementary Figure 1D), while free

doi:10.2217/NNM.12.73

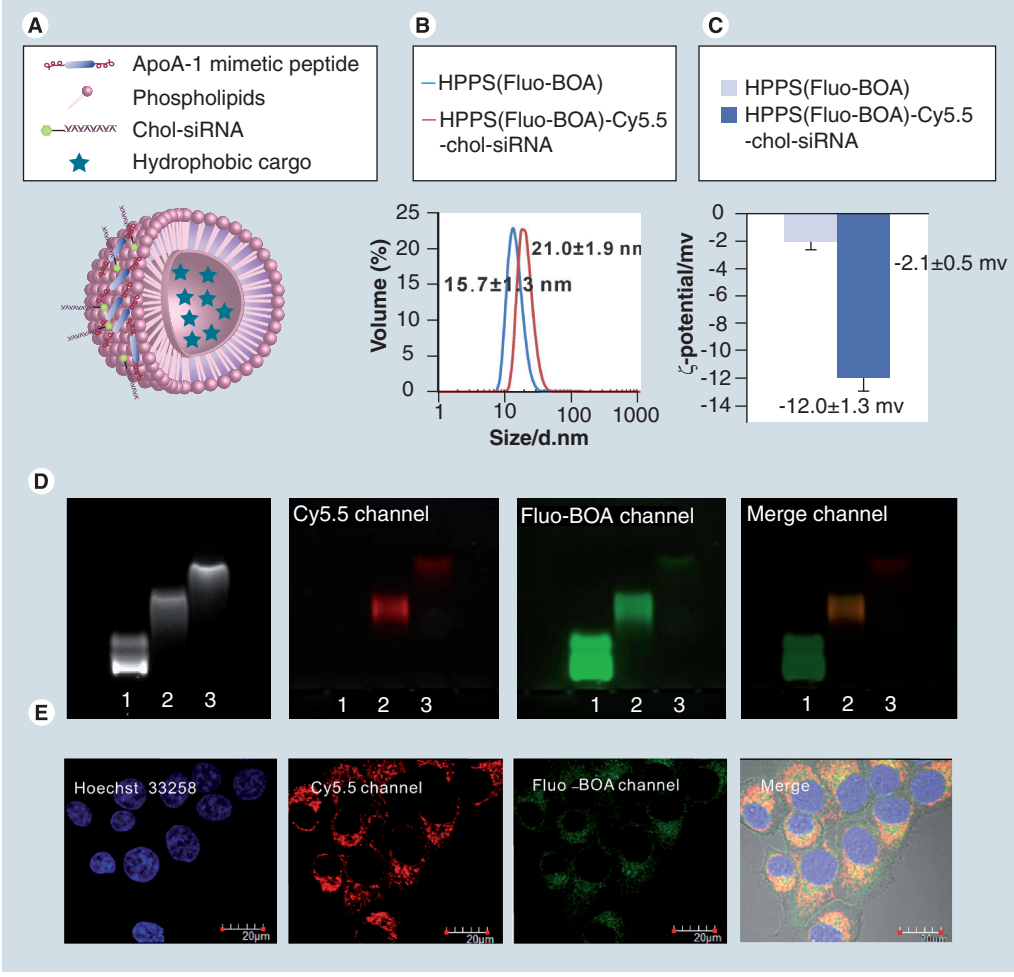

Figure 1. Characterization of HPPS(Fluo-BOA)-Cy5.5-chol-siRNA. (A) HPPS-chol-siRNA particles. **(B)** Size shift of HPPS after loading with chol-siRNA. **(C)** ζ-potential change of the HPPS particles after loading with chol-siRNA. **(D)** Agarose gel electrophoresis was used to check the integrity of HPPS-chol-siRNA particles. The first image represents agarose gel photographed by UV illumination, the others were fluorescence images. HPPS was labeled with Fluo-BOA (green signal) and chol-siRNA was labeled with Cy5.5 (red signal). Lane 1: HPPS(Fluo-BOA); lane 2: HPPS(Fluo-BOA)-Cy5.5-chol-siRNA; lane 3: free Cy5.5-chol-siRNA. **(E)** Confocal imaging of KB cells (SR-BI$^+$) incubated with HPPS(Fluo-BOA)-Cy5.5-chol-siRNA for 3 h. The cell nucleus was labeled with Hoechst 33258, HPPS was labeled with Fluo-BOA (green signal) and chol-siRNA was labeled with Cy5.5 (red signal).

Cy5.5-chol-siRNA degraded only after 1 h, confirming that HPPS can shield chol-siRNA from degradation in physiological conditions.

The *in vivo* behavior of HPPS-chol-siRNA

To elucidate the *in vivo* behavior of HPPS-chol-siRNA, the blood circulation time, biodistribution and tumor accumulation of chol-siRNA was determined and compared with free chol-siRNA in KB xenograft tumor-bearing nude mice. Chol-siRNA was labeled with Cy5.5 and tissue uptake monitored by Cy5.5 fluorescence. As shown in Supplementary Figure 2, the *in vivo* blood circulation of chol-siRNA was significantly altered by HPPS delivery. The circulation time of Cy5.5-chol-siRNA was determined to be 0.95 h and the blood clearance curve fits a one compartment model. When the same molecule was incorporated into HPPS, the clearance half-life of Cy5.5-chol-siRNA increased by a factor of 4 (3.9h) when the data was fit to a two compartment model. This indicated that HPPS-Cy5.5-chol-siRNA was quickly distributed from blood to body tissue and then slowly metabolized or excreted from the body. The increased circulation time improves the chance for HPPS-chol-siRNA to reach its target site. As a result, *in vivo* whole-body fluorescence imaging (Figure 2A) and *ex vivo* tissue fluorescence imaging (Figure 2B) showed that HPPS delivery totally changed the biodistribution pattern of Cy5.5-chol-siRNA. After 24 h systemic administration, the Cy5.5-chol-siRNA group only

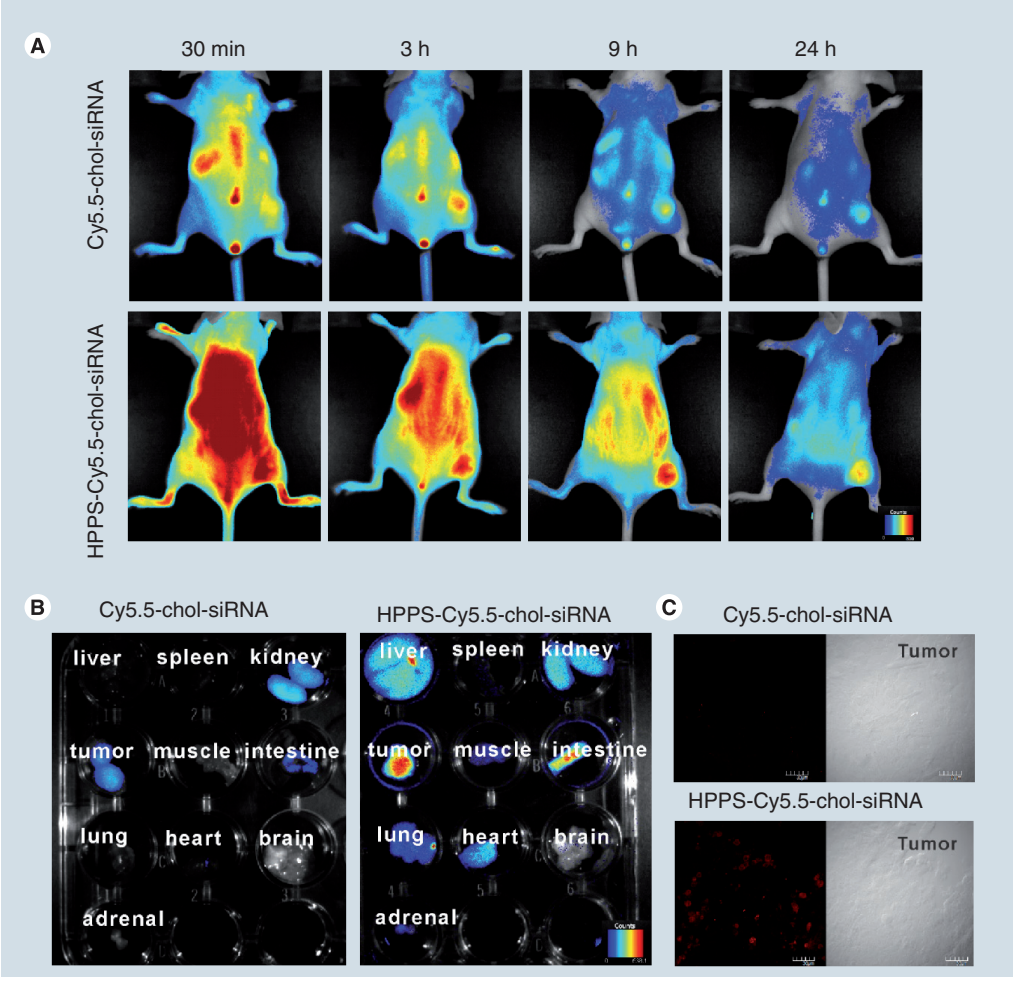

Figure 2. Fluorescence imaging of the *in vivo* behavior of HPPS-chol-siRNA. (A) *In vivo* whole-body fluorescence imaging of HPPS-chol-siRNA and free chol-siRNA using Cy5.5-labeled chol-siRNA. **(B)** *Ex vivo* organ imaging of HPPS-chol-siRNA and free chol-siRNA. **(C)** Confocal microscopy imaging of frozen tissue slides. All the images were taken under the same conditions between two groups at post 24 h injection.

showed weak fluorescence signal in the kidney, tumor and intestine, whereas the HPPS-Cy5.5-chol-siRNA group showed strong fluorescence in the tumor, liver and adrenal gland, which was consistent with HPPS particles (Supplementary Figure 3), suggesting that HPPS can stably carry siRNA for targeted delivery. The phospholipid scaffold without HDL-mimicking peptide was not used as a control for biodistribution comparison since it is not a stable formulation. In addition, this HPPS-driven biodistribution of siRNA was similar to recently reported siRNA biodistribution by HDL delivery [25], indicating that HPPS mimicked HDL function in delivery of siRNA *in vivo*. Compared with the Cy5.5-chol-siRNA group, the fluorescence signal in KB tumor of the HPPS-Cy5.5-chol-siRNA group was much intense (Figure 2A & B), suggesting that HPPS enhanced siRNA delivery into targeted KB tumor. In addition, confocal images of frozen tissue slices showed strong fluorescence signal inside tumor cells of the HPPS-Cy5.5-chol-siRNA group whereas minimal fluorescence signal was observed in tumor cells of the Cy5.5-chol-siRNA group (Figure 2C), confirming the HPPS-mediated enhanced siRNA delivery into tumor cells. Taken together, these studies demonstrate that HPPS prolonged the blood circulation time, improved *in vivo* biodistribution and facilitated the tumor uptake of chol-siRNA, thus improving siRNA delivery *in vivo*.

In vivo therapeutic efficacy of HPPS-cho-si-bcl-2

In our previous *in vitro* study [30], we have shown that *bcl-2* targeting chol-siRNA delivered by HPPS (HPPS-chol-si-bcl-2) enhanced *bcl-2* knockdown at both the gene and protein level when compared with free chol-si-bcl-2 group. Here, we continue to use *bcl-2* as a model target gene to investigate

doi:10.2217/NNM.12.73

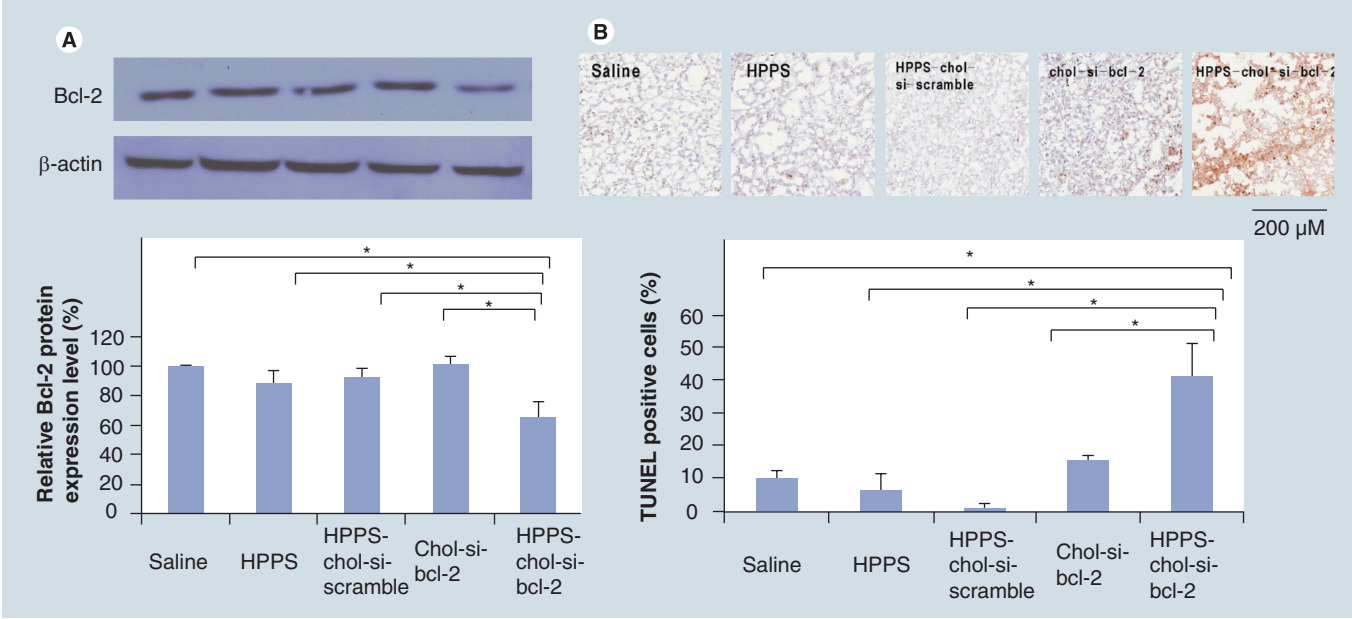

Figure 3. *In vivo* gene silencing efficacy. (A) Inhibition of Bcl-2 protein expression in KB tumor tissue by HPPS-chol-si-bcl-2 *in vivo*. KB xenograft tumor-bearing mice were systemically administered with saline (n = 6), HPPS (n = 3), HPPS-chol-si-scramble (n = 3), chol-si-bcl-2 (n = 6) and HPPS-chol-si-bcl-2 (n = 6), respectively, every other day for a total two doses. Bcl-2 protein expression level was assayed by Western blotting. **(B)** Evaluation of the induction of apoptosis by HPPS-chol-si-bcl-2 using TUNEL staining in KB tumor tissue. Results are shown as ratios of TUNEL-positive cells to total cells (n = 3).
Error bars represent standard deviation. The student's t-test (two tailed) was used to determine significant differences in Western blotting and TUNEL staining and p-values less than 0.05 were considered significant (*$p < 0.05$).

the *in vivo* therapeutic efficacy of chol-siRNA by HPPS delivery. KB tumor-bearing mice were treated with HPPS-chol-si-bcl-2 (n = 6) once every 2 days for 4 days by intravenous injection. Saline (n = 6), HPPS (n = 3), HPPS-chol-si-scramble (HPPS loaded with scramble bcl-2 siRNA; n = 3) and chol-si-bcl-2 alone (n = 6) were also given as controls. The tumor volume was monitored before treatment and 4 days after the first dose, and then all tumors were excised for determining therapeutic response. Upon HPPS-chol-si-bcl-2 treatment, Bcl-2 protein expression in KB tumor was decreased by 34%, whereas no significant decrease in protein expression was observed for the saline, HPPS alone, chol-si-bcl-2 and HPPS-chol-si-scramble control groups (Figure 3A). Since downregulation of the Bcl-2 protein could induce apoptosis [34,35], we next examined the apoptosis of tumor tissue by using the TUNEL assay. As shown in Figure 3B, HPPS-chol-si-bcl-2 induced much enhanced apoptosis in tumor tissue (41.9% of total tissue cells) than chol-si-bcl-2 alone (16.1%); and no significant apoptosis was observed in saline, HPPS and HPPS-chol-si-scramble controls. These data demonstrate that HPPS improved the therapeutic efficacy of chol-siRNA in targeted tumor. More importantly, after the two-dose regime, the relative tumor volume increase of the control groups were 198% (saline), 316% (HPPS), 214% (HPPS-chol-si-scramble) and 233% (chol-si-bcl-2), whereas the relative tumor volume of the HPPS-chol-si-bcl-2 treatment group increased only 42% (Figure 4). This result confirmed that there was a significant tumor growth inhibition by using this siRNA delivery strategy.

Collectively, these *in vivo* antitumor studies provide convincing evidence that HPPS is not only able to efficiently deliver siRNA to target tissue, but is also capable of facilitating the gene knockdown of siRNA in tumor and improve antitumor efficacy.

The adverse effect of HPPS-chol-si-bcl-2

To evaluate whether HPPS-chol-si-bcl-2 induced any adverse effect during treatment, healthy BALB/c mice were subjected to the same HPPS-chol-si-bcl-2 treatment as the functional studies (*vide supra*) and their behavioral, physical and biochemical effects were then assessed. Mice injected with 200 μl of saline were used as controls. During the treatment regimen, no abnormalities in behavior or significant changes in body weight were observed in the HPPS-chol-si-bcl-2 treated group. The weight of the saline control group changed from 20.1 ± 0.7 to 20.3 ± 1.0 g and that of the HPPS-chol-si-bcl-2 group changed from

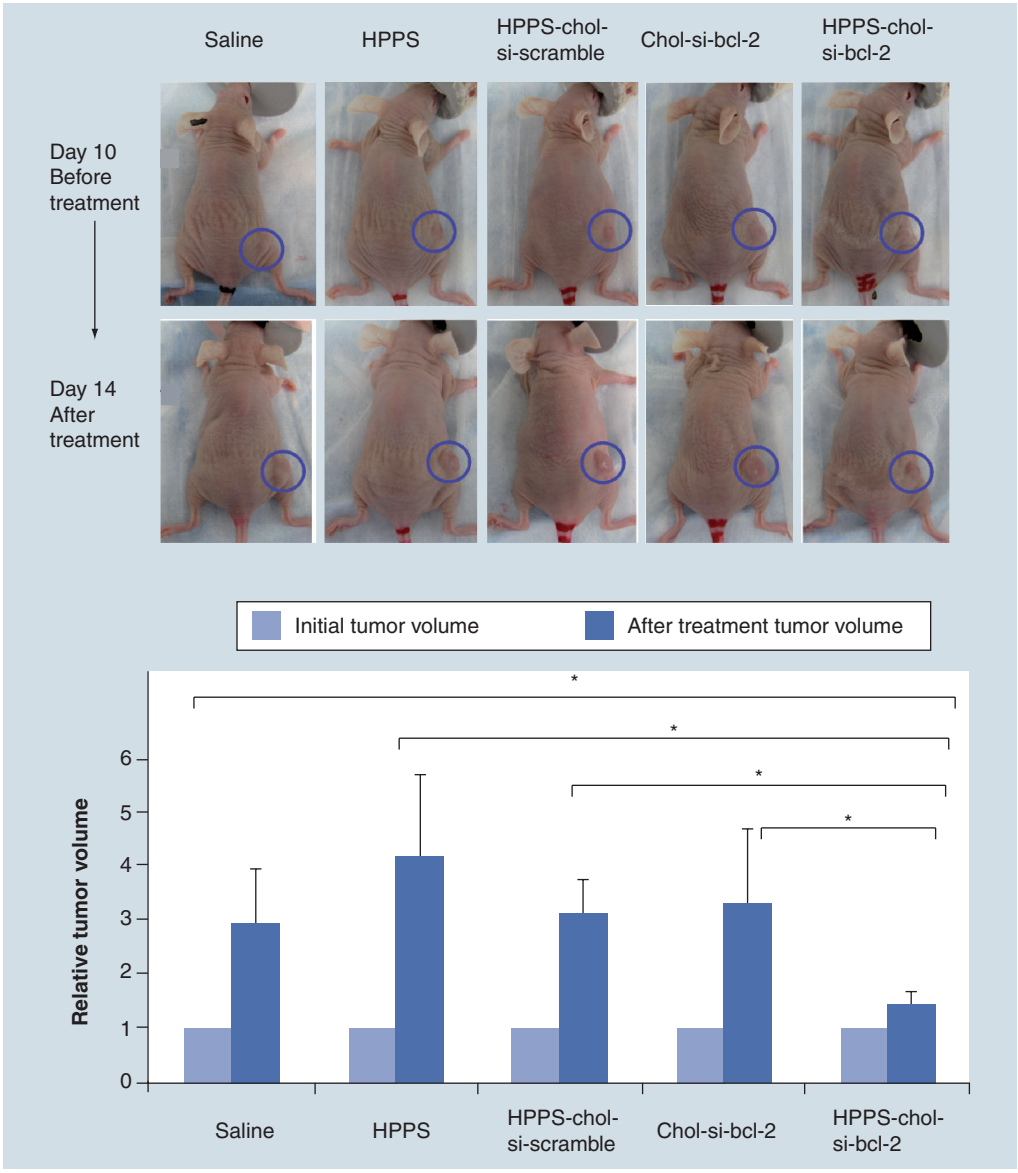

Figure 4. *In vivo* anticancer effect of systemic administration of HPPS-chol-si-bcl-2 in KB xenograft tumor model. KB xenograft tumor-bearing mice were systemically administered with saline (n = 6), HPPS (n = 3), HPPS-chol-si-scramble (n = 3), chol-si-bcl-2 (n = 6) and HPPS-chol-si-bcl-2 (n = 6), respectively, every other day for a total two doses. Tumor volume was measured at day 10 before treatment and day 14 after treatment, respectively, by blind method.
Error bars represent standard deviation. The student's t-test (two tailed) was used to determine significance and p-values less than 0.05 were considered significant (*$p < 0.05$).

20.1 ± 0.8 to 20.2 ± 0.7 g. When compared with saline controls, the HPPS-chol-si-bcl-2 treatment group did not show any measurable adverse effect on liver function (alanine aminotransferase: 34.0 ± 2.5 U/l; alkaline phosphatase: 93.5 ± 14.2 U/l; and total bilirubin: 3.0 ± 0.8 µmol/l) as well as renal function (urea nitrogen: 6.6±1.0 mmol/l; creatinine: 19.2 ± 0.7 µmol/l; and globulin: 19.0 ± 1.6 g/l) (Figure 5). In addition, there was no significant difference in histology between HPPS-chol-si-bcl-2 groups and saline controls, and all organs including hearts, livers, spleens, lungs and kidneys did not show any significant pathologic abnormality. These data indicate there was no adverse effect of HPPS-chol-si-bcl-2 during treatment.

Discussion

In this study we investigated the use of HPPS nanoparticles for siRNA delivery *in vivo*. Each HPPS nanoparticle stably incorporated chol-siRNAs and the resulting nanoparticles can shield siRNA from degradation in serum

doi:10.2217/NNM.12.73

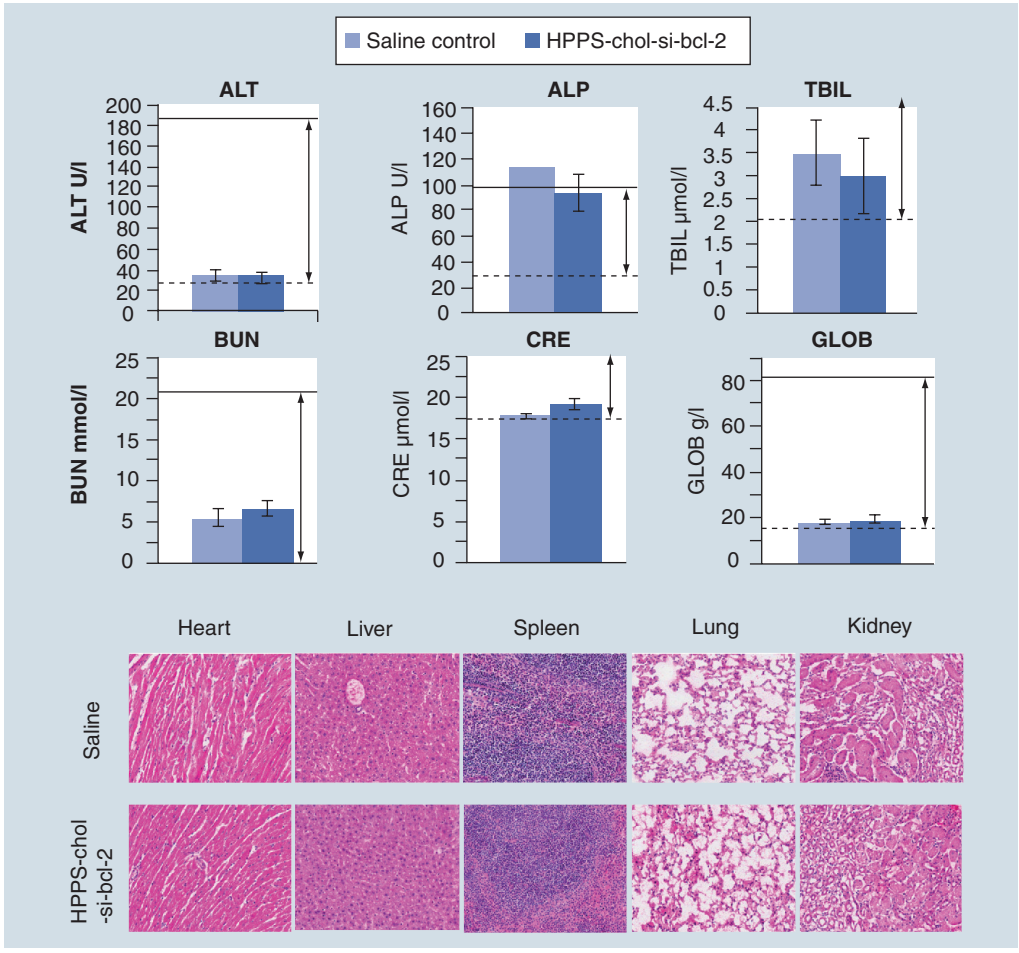

Figure 5. The evaluation of the adverse effect of HPPS-chol-si-bcl-2 on healthy BALB/c mice.
The healthy BALB/c mice (female, 6–7 weeks old) were intravenously administered with 10 mg/kg HPPS-chol-si-bcl-2 (n = 4) every other day for a total two doses. Liver function (ALT, ALP, TBIL) and renal function (BUN, CRE, GLOB) were detected at 4 days after injection, and all the organs were excised at 4 days after injection. Error bars represent standard deviation. The Student's t-test (two tailed) was used to determine significance, and p-values less than 0.05 were considered significant.
ALT: Alanine aminotransferase; ALP: Alkaline phosphatase; BUN: Urea nitrogen; CRE: Creatinine; GLOB: Globulin; TBIL: Total bilirubin.

(Supplementary Figure 2). After systemic administration in KB tumor-bearing mice, HPPS prolonged siRNA circulation in the bloodstream by a factor of 4, improved its biodistribution and facilitated its uptake in SR-BI overexpressed KB tumors. These improvements are attributed to the HDL-like structural and functional characteristics of HPPS nanoparticles. The favorable small size (20–30 nm) of HPPS can enable the nanoparticle to penetrate through the restricted interfibrillar openings (<40 nm) commonly present in solid tumors [36] while at the same time allowing it to escape kidney filtration (Figure 2B). Besides the size effect, the SR-BI targeting of HPPS also played an important role in efficient delivery of siRNA, evidenced by the good correlation between the accumulation of HPPS-chol-siRNA and the expression of SR-BI in different tissues of the KB-bearing mice. KB tumors and some normal organs including the liver, adrenal gland and other steroidogenic tissues expressing high levels of SR-BI receptor [37–39] showed strong Cy5.5 fluorescence at 24 h after injection of HPPS-Cy5.5-chol-siRNA (Figure 2B). Efficient delivery of siRNA to tumors *in vivo* not only requires good tumor accumulation, but also requires its efficient transportation into the cytoplasm of targeted cells where siRNAs are recognized and can associate with the RNA-induced silencing complex to perform their function for gene knockdown. The direct cytosolic delivery of siRNA by HPPS allows siRNA to reach its action site of cytosol, thus bypassing the detrimental endosomal trafficking, which normally induce siRNA degradation in lysosomes. It has been demonstrated that HPPS is a safe nanocarrier evidenced by the

Executive summary

The integrity and stability of HPPS-chol-siRNA nanoparticles

- High-density lipoprotein-mimicking peptide–phospholipid scaffold (HPPS) core payload and siRNA payload were both transported into the cytoplasm of cells by the SR-BI-mediated uptake pathway and the integrity and stability of HPPS(Fluo-BOA)-Cy5.5-chol-siRNA was confirmed *in vitro*.

***The behavior of HPPS-chol-siRNA* in vivo**

- HPPS prolonged the blood circulation time, improved *in vivo* biodistribution and facilitated the tumor uptake of chol-siRNA, thus improving siRNA delivery *in vivo*.

In vivo *therapeutic efficacy of HPPS-cho-si-bcl-2*

- HPPS is not only able to efficiently deliver siRNA to target tissue, but is also capable of facilitating the gene knockdown of siRNA in tumors and improving antitumor efficacy.

The adverse effect of HPPS-chol-si-bcl-2

- No adverse effects of HPPS-chol-si-bcl-2 during treatment were reported.

absence of adverse effects when 2000 mg/kg of HPPS was administered intravenously [29]. This study further proved that HPPS is a safe delivery vehicle for efficient RNAi therapeutics since no adverse effect of HPPS-chol-si-bcl-2 was detected during treatment (Figure 5).

Increased SR-BI expression has been reported in many cancer cell lines including: prostate adenocarcinoma [40], cervical carcinoma, breast cancer, ovary adenocarcinoma [21,41,42], lung cancer cell lines [43] and hepatoma cell lines [44,45], indicating the potential application of HPPS for targeted delivery of different siRNAs of choice for personalized cancer treatment. For anticancer therapy, simple knockdown of the *bcl-2* gene may not be sufficient to achieve effective antitumor activity since the apoptosis pathway is very complicated, with other proteins such as Bcl-xL, Mcl-1, Bax and BH3 playing a role in whether apoptosis occurs [34]. Several studies have demonstrated that combination of *bcl-2* gene knockdown with chemotherapy achieved enhanced therapeutic efficacy in multidrug-resistant cancer cells [46–50]. The suppression of Bcl-2 expression in tumors could increase chemotherapeutic efficacy. In our previous study [29], we successfully employed HPPS for targeted delivery of the chemotherapeutic drug, paclitaxel oleate (PTXOL). The resulting HPPS(PTXOL) particles not only induced effective therapeutic activity to targeted cells, but also attenuated cytotoxicity of anticancer drugs to nontargeted cells. In this study, we developed a dual cargo-loaded particle, HPPS(Fluo-BOA)-Cy5.5-chol-siRNA, where Fluo-BOA hydrophobic dye was loaded into the HPPS core and chol-siRNA was loaded into the HPPS surface membrane. The integrity and stability of the resulting particle had been demonstrated and its capability to direct cytosolic delivery of core-loaded Fluo-BOA and surface-loaded siRNA had also been validated. This suggests the potential utility of HPPS for combination therapy by co-delivery of chemotherapeutic drug in the core and siRNA on the surface.

Conclusion

In summary, HPPS was capable of prolonging the circulation time of chol-siRNA in blood, improved the biodistribution pattern and facilitated the uptake of chol-siRNA in the KB xenograft tumor model. For functional study, HPPS-chol-si-bcl-2 nanoparticles down regulated the Bcl-2 protein and enhanced induction of apoptosis. It also delayed tumor growth when compared with chol-si-bcl-2. Furthermore, no adverse effect was observed during the treatment. Many features of HPPS, such as the ideal small size (10–25 nm), cytosolic delivery fate, built-in SR-BI targeting and good biocompatibility, point to its potential usage as an ideal siRNA delivery vehicle.

Future perspective

As a good siRNA delivery vehicle, HPPS can be widely used in targeted delivery of different siRNAs of choice for personalized cancer treatment. HPPS provides a promising strategy for combination therapy in the future by loading chemotherapeutic drug into the HPPS core and siRNA on surface membrane. HPPS may also influence other disease treatments, such as that for liver disease and cardiovascular disease due to high SR-BI expression in the liver, steroidogenic tissues and circulating macrophages [39].

Financial & competing interests disclosure

This study was conducted with the support of the Canadian Institutes of Health Research, the Ontario Institute for Cancer Research through funding provided by the Government of Ontario, the China-Canada Joint Health Research Initiative (CIHR CCI-102936 & NSFC-30911120489), the Natural Sciences and Engineering Research Council of Canada, and the Joey and Toby

 doi:10.2217/NNM.12.73

Tanenbaum/Brazilian Ball Chair in Prostate Cancer Research. G Zheng is associated with DLVR Therapeutics Inc. and is a scientific co-founder of DLVR, a start-up company based on the HPPS technology. The authors have no other relevant affiliations or financial involvement with any organization or entity with a financial interest in or financial conflict with the subject matter or materials discussed in the manuscript apart from those disclosed.

No writing assistance was utilized in the production of this manuscript.

References

Papers of special note have been highlighted as:
▪ of interest

1 Whitehead KA, Langer R, Anderson DG. Knocking down barriers: advances in siRNA delivery. *Nat. Rev. Drug Discov.* 8(2), 129–138 (2009).

2 Castanotto D, Rossi JJ. The promises and pitfalls of RNA-interference-based therapeutics. *Nature* 457(7228), 426–433 (2009).

3 Eguchi A, Meade BR, Chang YC *et al.* Efficient siRNA delivery into primary cells by a peptide transduction domain–dsRNA binding domain fusion protein. *Nature Biotechnol.* 27(6), 567–571 (2009).

4 Kortylewski M, Swiderski P, Herrmann A *et al. In vivo* delivery of siRNA to immune cells by conjugation to a TLR9 agonist enhances antitumor immune responses. *Nature Biotechnol.* 27(10), 925–932 (2009).

5 Dassie JP, Liu XY, Thomas GS *et al.* Systemic administration of optimized aptamer-siRNA chimeras promotes regression of PSMA-expressing tumors. *Nature Biotechnol.* 27(9), 839–849 (2009).

6 Peer D, Park EJ, Morishita Y, Carman CV, Shimaoka M. Systemic leukocyte-directed siRNA delivery revealing cyclin D1 as an anti-inflammatory target. *Science* 319(5863), 627–630 (2008).

7 Soutschek J, Akinc A, Bramlage B *et al.* Therapeutic silencing of an endogenous gene by systemic administration of modified siRNAs. *Nature* 432(7014), 173–178 (2004).

8 Akinc A, Zumbuehl A, Goldberg M *et al.* A combinatorial library of lipid-like materials for delivery of RNAi therapeutics. *Nature Biotechnol.* 26(5), 561–569 (2008).

9 Akinc A, Goldberg M, Qin J *et al.* Development of lipidoid-siRNA formulations for systemic delivery to the liver. *Mol. Ther.* 17(5), 872–879 (2009).

10 Frank-Kamenetsky M, Grefhorst A, Anderson NN *et al.* Therapeutic RNAi targeting PCSK9 acutely lowers plasma cholesterol in rodents and LDL cholesterol in nonhuman primates. *Proc. Natl Acad. Sci USA* 105(33), 11915–11920 (2008).

11 Love KT, Mahon KP, Levins CG *et al.* Lipid-like materials for low-dose, *in vivo* gene silencing. *Proc. Natl Acad. Sci USA* 107(5), 1864–1869 (2010).

12 Liu G, Xie J, Zhang F *et al.* N-Alkyl-PEI-functionalized iron oxide nanoclusters for efficient siRNA delivery. *Small* 7(19), 2742–2749 (2011).

13 Qi L, Gao X. Quantum dot-amphipol nanocomplex for intracellular delivery and real-time imaging of siRNA. *ACS Nano* 2(7), 1403–1410 (2008).

14 De Fougerolles AR. Delivery vehicles for small interfering RNA *in vivo*. *Hum. Gene Ther.* 19(2), 125–132 (2008).

15 Sato Y, Murase K, Kato J *et al.* Resolution of liver cirrhosis using vitamin A-coupled liposomes to deliver siRNA against a collagen-specific chaperone. *Nature Biotechnol.* 26(4), 431–442 (2008).

16 Kuwahara H, Nishina K, Yoshida K *et al.* Efficient *in vivo* delivery of siRNA into brain capillary endothelial cells along with endogenous lipoprotein. *Mol. Ther.* 19(12), 2213–2221 (2011).

17 Hartono SB, Gu W, Kleitz F *et al.* Poly-L-lysine functionalized large pore cubic mesostructured silica nanoparticles as biocompatible carriers for gene delivery. *ACS Nano* 6(3), 2104–2117 (2012).

18 Yang XZ, Du JZ, Dou S, Mao CQ, Long HY, Wang J. Sheddable ternary nanoparticles for tumor acidity-targeted siRNA delivery. *ACS Nano* 6(1), 771–781 (2012).

19 Alvarez-Erviti L, Seow Y, Yin H, Betts C, Lakhal S, Wood MJ. Delivery of siRNA to the mouse brain by systemic injection of targeted exosomes. *Nature Biotechnol.* 29(4), 341–345 (2011).

20 Jin H, Lovell JF, Chen J *et al.* Mechanistic insights into LDL nanoparticle-mediated siRNA delivery. *Bioconjug. Chem.* 23(1), 33–41 (2011).

21 Lacko AG, Nair M, Prokai L, Mcconathy WJ. Prospects and challenges of the development of lipoprotein-based formulations for anti-cancer drugs. *Exp. Opin. Drug Deliv.* 4(6), 665–675 (2007).

22 Ng KK, Lovell JF, Zheng G. Lipoprotein-inspired nanoparticles for cancer theranostics. *Acc. Chem. Res.* 44(10), 1105–1113 (2011).

23 Zheng G, Chen J, Li H, Glickson JD. Rerouting lipoprotein nanoparticles to selected alternate receptors for the targeted delivery of cancer diagnostic and therapeutic agents. *Proc. Natl Acad. Sci USA* 102(49), 17757–17762 (2005).

24 Acton S, Rigotti A, Landschulz KT, Xu S, Hobbs HH, Krieger M. Identification of scavenger receptor SR-BI as a high density lipoprotein receptor. *Science* 271(5248), 518–520 (1996).

▪ **Discovery of scavenger receptor class B type 1 as a receptor for high-density lipoprotein (HDL).**

25 Wolfrum C, Shi S, Jayaprakash KN *et al.* Mechanisms and optimization of *in vivo* delivery of lipophilic siRNAs. *Nature Biotechnol.* 25(10), 1149–1157 (2007).

▪ **First paper on *in vivo* delivery of siRNA using HDL.**

26 Kuwahara H, Nishina K, Yoshida K *et al.* Efficient *in vivo* delivery of sirna into brain capillary endothelial cells along with endogenous lipoprotein. *Mol. Ther.* 19(12), 2213–2221 (2011).

27 Shahzad MM, Mangala LS, Han HD *et al.* Targeted delivery of small interfering RNA using reconstituted high-density lipoprotein nanoparticles. *Neoplasia* 13(4), 309–319 (2011).

28 Zhang Z, Cao W, Jin H *et al.* Biomimetic nanocarrier for direct cytosolic drug delivery. *Angew Chem. Int. Ed. Engl.* 48(48), 9171–9175 (2009).

29 Yang M, Chen J, Cao W *et al.* Attenuation of nontargeted cell-kill using a high-density lipoprotein-mimicking peptide – phospholipid nanoscaffold. *Nanomedicine (Lond).* 6(4), 631–641 (2011).

30 Yang M, Jin H, Chen J *et al.* Efficient cytosolic delivery of siRNA using HDL-mimicking nanoparticles. *Small* 7(5), 568–573 (2011).

▪ **First paper that validated cytosolic delivery of siRNA using HDL-mimicking peptide phospholipids nanoscaffold (HPPS) *in vitro*.**

31 Krieger M, Smith LC, Anderson RG *et al.* Reconstituted low density lipoprotein: a vehicle for the delivery of hydrophobic fluorescent probes to cells. *J. Supramol. Struct.* 10(4), 467–478 (1979).

32 Zhang Z, Chen J, Ding L *et al.* HDL-mimicking peptide-lipid nanoparticles with improved tumor targeting. *Small* 6(3), 430–437 (2010).

33 Wijsman JH, Jonker RR, Keijzer R, Van De Velde CJ, Cornelisse CJ, Van Dierendonck JH. A new method to detect apoptosis in paraffin sections: *in situ* end-labeling of

fragmented DNA. *J. Histochem. Cytochem.* 41(1), 7–12 (1993).

34 Adams JM, Cory S. The Bcl-2 protein family: arbiters of cell survival. *Science* 281(5381), 1322–1326 (1998).

35 Huang Z. Bcl-2 family proteins as targets for anticancer drug design. *Oncogene* 19(56), 6627–6631 (2000).

36 Pluen A, Boucher Y, Ramanujan S *et al.* Role of tumor-host interactions in interstitial diffusion of macromolecules: cranial vs. subcutaneous tumors. *Proc. Natl Acad. Sci USA* 98(8), 4628–4633 (2001).

37 Al-Jarallah A, Trigatti BL. A role for the scavenger receptor, class B type I in high density lipoprotein dependent activation of cellular signaling pathways. *Biochim. Biophys. Acta* 1801(12), 1239–1248 (2010).

38 Krieger M. Scavenger receptor class B type I is a multiligand HDL receptor that influences diverse physiologic systems. *J. Clin. Invest.* 108(6), 793–797 (2001).

39 Krieger M. Charting the fate of the 'good cholesterol': identification and characterization of the high-density lipoprotein receptor SR-BI. *Ann. Rev. Biochem.* 68, 523–558 (1999).

40 Mooberry LK, Nair M, Paranjape S, Mcconathy WJ, Lacko AG. Receptor mediated uptake of paclitaxel from a synthetic high density lipoprotein nanocarrier. *J. Drug Target.* 18(1), 53–58 (2010).

41 Mcconathy WJ, Nair MP, Paranjape S, Mooberry L, Lacko AG. Evaluation of synthetic/reconstituted high-density lipoproteins as delivery vehicles for paclitaxel. *Anticancer Drugs* 19(2), 183–188 (2008).

42 Kader A, Pater A. Loading anticancer drugs into HDL as well as LDL has little affect on properties of complexes and enhances cytotoxicity to human carcinoma cells. *J. Control. Release* 80(1–3), 29–44 (2002).

43 Hrzenjak A, Reicher H, Wintersperger A *et al.* Inhibition of lung carcinoma cell growth by high density lipoprotein-associated alpha-tocopheryl-succinate. *Cel. Mol. Life Sci.* 61(12), 1520–1531 (2004).

44 Krasteva V, Brodeur MR, Tremblay FL, Falstrault L, Brissette L. Apolipoprotein C-I reduces cholesteryl esters selective uptake from LDL and HDL by binding to HepG2 cells and lipoproteins. *Biochim. Biophys. Acta* 1801(1), 42–48 (2010).

45 Rhainds D, Bourgeois P, Bourret G, Huard K, Falstrault L, Brissette L. Localization and regulation of SR-BI in membrane rafts of HepG2 cells. *J. Cell Sci.* 117(Pt 15), 3095–3105 (2004).

46 Saad M, Garbuzenko OB, Minko T. Co-delivery of siRNA and an anticancer drug for treatment of multidrug-resistant cancer. *Nanomedicine (Lond).* 3(6), 761–776 (2008).

47 George J, Banik NL, Ray SK. Bcl-2 siRNA augments taxol mediated apoptotic death in human glioblastoma U138MG and U251MG cells. *Neurochem. Res.* 34(1), 66–78 (2009).

48 Chen AM, Zhang M, Wei D *et al.* Co-delivery of doxorubicin and Bcl-2 siRNA by mesoporous silica nanoparticles enhances the efficacy of chemotherapy in multidrug-resistant cancer cells. *Small* 5(23), 2673–2677 (2009).

49 Meng H, Liong M, Xia T *et al.* Engineered design of mesoporous silica nanoparticles to deliver doxorubicin and P-glycoprotein siRNA to overcome drug resistance in a cancer cell line. *ACS Nano* 4(8), 4539–4550 (2010).

50 Pandyra AA, Berg R, Vincent M, Koropatnick J. Combination silencer RNA (siRNA) targeting Bcl-2 antagonizes siRNA against thymidylate synthase in human tumor cell lines. *J. Pharmacol. Exper. Therap.* 322(1), 123–132 (2007).

doi:10.2217/NNM.12.73